Temperature measurements near the heating surface at high heat fluxes in pool boiling of 2-propanol/water mixtures

Hiroto Sakashita *

Division of Energy and Environmental Systems, Graduate School of Engineering,

Hokkaido University, North 13 West 8, Kita-ku, Sapporo 060-8628, Japan

* Corresponding author. Tel.: +81 11 706 6664, Fax.: +81 11 706 6664

E-mail address: saka@eng.hokudai.ac.jp

Highlights

The temperatures near the heating surface were measured using a micro thermocouple at high heat fluxes

The local concentrations of 2-propanol were estimated based on the measured local temperatures

The distributions of 2-propanol concentration have strong non-uniformities in the vertical and radial directions

Abstract

To examine the mechanism of CHF enhancement with binary mixtures, this paper measured local temperatures close to a heating surface using a micro-thermocouple at high heat fluxes for pool boiling of a 3mol% of 2-propanol/water mixture on an upward-facing 12mm diameter circular surface. The variations in temperature traces measured at various locations above the heating surface indicate that the distributions of 2-propanol concentration have strong non-uniformities in the vertical and radial directions: 2-propanol concentration is higher in the vicinity of the heating surface at the central part of the heating surface and lower in the periphery of the heating surface. The local concentration of 2-propanol was determined based on the assumption that low peak values of temperature fluctuations correspond to the local saturation temperatures of the mixture. This assumption enabled a quantitative representation of the concentration distributions in the vertical and radial directions. The variations in the surface tension of the mixture were evaluated based on the deduced local values of the saturation temperature and the composition of the mixture. It was found that near the heating surface the surface tension increases steeply in the direction of the heating surface, suggesting that intensive Marangoni convection is induced at the liquid/vapor interface near the heating surface.

Key Words: Binary mixture, Pool boiling, Micro-thermocouple, Temperature measurement, Concentration distribution, Critical heat flux

1. Introduction

The CHF in pool boiling is often enhanced when binary mixtures are used as working fluids. This characteristic of binary mixtures has potential applications for coolants of thermal devices with high heat flux components. A number of experimental and theoretical studies have been conducted for the CHF of binary mixtures, and various mechanistic models responsible for the CHF enhancement have been proposed. The proposed models are categorized into the following two types.

A first category is based on increases in the effective subcooling around vapor bubbles. In the boiling of mixtures, the concentration of less volatile component around the vapor bubbles becomes richer than that of the bulk liquid due to preferential evaporation of the more volatile component. As a result, the temperature of the liquid near the liquid-vapor interface becomes higher than the saturation temperature (bubble point temperature) of the bulk liquid. This situation is similar to that of subcooled boiling with a single component fluid, and is a cause of the CHF increase. Based on this idea, McEligot [1], and Reddy and Lienhard [2] have proposed empirical equations to predict the CHF of binary mixtures.

The second category of proposed CHF enhancement models is based on the Marangoni effect occurring at the liquid-vapor interface. In the boiling of binary mixtures, evaporation of the more volatile component from the liquid-vapor interface is more intensive near the heating surface, and hence, concentration of the more volatile component in the liquid phase adjacent to the interface decreases toward the heating surface. This yields a surface tension gradient according to the concentration distribution along the liquid-vapor interface. For the positive mixtures where the more volatile component has the lower surface tension, therefore, Marangoni convection is induced toward the heating surface,

and may be a cause of the CHF enhancement. Hovestreudt [3], Fujita and Bai [4], Mcgillis and Carey [5], and Yagov [6] proposed empirical equations for the CHF incorporating the Marangoni effect, although the assumed CHF models are different in the different studies: a bubble merger model [3], a dry-spot model [4,6], and Zuber's instability model [5], respectively.

As above, there are a number of studies on the CHF of binary mixtures, and details of the mechanism of the CHF enhancement are not fully understood. To examine this phenomenon experimentally, the author here and coworkers [7] have investigated the CHF for 2-propanol/water mixtures during pool boiling on an upward-facing heating surface under atmospheric pressure. They measured the liquid-vapor behaviors near the heating surface using a conductance probe, and determined the thickness of the liquid layer (a so called macrolayer) formed beneath large vapor masses from the location of disappearance of vapor mass signals. Through these measurements, it was established that: (1) at a 2-propanol concentration of around 3.0 to 4.7 mol% the CHF of 2-propanol/water mixtures is enhanced 1.7 times compared with the CHF of water, (2) the macrolayer thicknesses of a 3.0 mol% 2-propanol/water mixture formed at the center of the heating surface are considerably thicker than those of water at heat fluxes close to the CHF of water, (3) the macrolayer thicknesses of the 3.0 mol% 2-propanol/water mixture show a non-uniform distribution in the radial direction, thicker at the central area and thinner near the periphery of the heating surface, and (4) the change in the macrolayer thickness with the concentration of 2-propanol is similar to that in the CHF: with increasing concentrations of 2-propanol, the macrolayer thickness increases, to reach a maximum at around 3.0 to 4.7 mol% and then decreases.

The above results, (1) to (4), suggest that the formation of a thicker macrolayer at the central area of the heating surface is responsible for the CHF

enhancement in 2-propanol/water mixtures. This mechanism is different from the mechanisms assumed in existing models [1-6], however, the formation of thicker macrolayers and the radial non-uniformity of the macrolayer thickness are likely caused by non-uniformities in the 2-propanol concentration in the vicinity of the heating surface as is suggested by the existing models. Therefore, information of local concentrations of 2-propanol close to a heating surface at high heat fluxes is vital to clarify the CHF enhancement mechanism for 2-propanol/water mixtures.

Attempts to estimate the local concentrations of binary mixtures in pool boiling have been conducted by Van Stralen and Sluyter [8], Copper and Stone [9], and Utaka and Sai [10] at low heat fluxes (the isolated bubble region). These studies measured the temperatures inside the isolated bubbles detached from the heating surface, and showed that the temperature inside the bubbles is higher than the saturation temperature of the surrounding bulk liquid. (Concentration of the more volatile component is lower in the bubble than in the bulk liquid). However, there have been no attempts addressing an evaluation of the concentration of binary mixtures in the vicinity of the heating surface at high heat flux conditions. The study here measured the local temperatures close to a heating surface with a micro-thermocouple at high heat fluxes for pool boiling of 3 mol% 2-propanol/water mixture on an upward-facing surface, and estimated the vertical and radial distributions of the 2-propanol concentrations based on the measured local temperatures.

2. Experiments

2.1 Experimental apparatus

The experiments were carried out in saturated pool boiling of 3mol% 2-propanol/water mixture at atmospheric pressure. Fig.1 shows the experimental apparatus, which is the same as that used in the previous study [7], except for a

thermocouple probe and temperature measurement arrangement. The heating surface is the upper end of a cylindrical 12 mm diameter copper block. A 0.5 mm thick stainless steel flange was silver-soldered around the copper heating surface. The surfaces of the copper and the surrounding flange were machined to be flush, and then Ni was plated over the two surfaces to avoid nucleation of bubbles at the interface between the copper surface and the flange. The surface heat flux and surface temperature were determined with two 0.5 mm diameter thermocouples, embedded in the copper block 4 and 12 mm below the surface. The boiling vessel is made of Pyrex glass with an inner diameter of 150 mm. Two auxiliary heaters were installed in the boiling vessel and were used for heating and degassing the mixture. The liquid temperature during the measurements was monitored with a sheathed thermocouple placed 7 mm above the heating surface and 25 mm from the center of the heating surface, the temperature measured in this manner was defined as the saturation temperature of the mixture.

Fig. 2-(a) shows a photo of the micro-thermocouple used in the present experiment, and Fig. 2-(b) is an enlarged illustration of the tip of the micro-thermocouple. The micro-thermocouple was manufactured from 25 μm diameter chromel and alumel wires, insulated with polyimide resin except at the junction. The two parallel wires were welded at the ends, and finished as a needle type thermocouple with a v-shaped junction. The dimensions of the junction part are about 30 μm long and 50 μm in diameter, as shown in Fig.2-(b). This micro-thermocouple was inserted in a conical capillary quarts tube with very low thermal expansion coefficient, and exposed about 2 mm from the tip of the quarts tube, as shown in Fig.2-(a). The time constant of the thermocouple probe was investigated in [11] using temperature traces measured during subcooled pool boiling of water, and estimated as about 0.7 ms for the measurement in liquid phase. The micro-thermocouple probe was connected to a three-dimensional

moving stage with a positional accuracy of 0.5 μm in the vertical direction and 10 μm in the horizontal direction. The noise level in the output signal of the thermocouple was less than 0.2 K, and no process to remove the noise from the signals was included.

The voltage of the output signals from the micro-thermocouple was amplified 100-fold and sent to a PC through an A/D converter. The height of the thermocouple tip was calibrated by detecting the electrical contact between the tip of the micro-thermocouple and the heating surface using a short detection circuit.

2.2 Phase equilibrium of 2-propanol/water mixtures

Fig. 3 shows the phase equilibrium of 2-propanol/water mixtures. For the boiling of the mixture with a 2-propanol mole fraction of x, the saturation temperature of the bulk liquid is given by T_{bp} (Point A). Near the heating surface, however, local saturation temperatures become higher than T_{bp} due to preferential evaporation of 2-propanol and can rise to a maximum value $T_{bp,max}$ (Point B). Fig.4 enlarges the phase equilibrium of the region of the mole fraction from 0 to 0.1, to show the phase equilibrium around the 3 mol% 2-propanol/water mixture used in the present experiment more clearly. The saturation temperature, T_{bp}, of the 3 mol% mixture is 89.1℃, with the maximum saturation temperature, $T_{bp,max}$, is 99.7 ℃. The mole fractions of the 2-propanol in the liquid and vapor phases at this maximum saturation temperature become 0.034 % and 3 % respectively, as shown at points C and B in Fig.4.

3. Results and Discussion

3.1 Boiling curves and boiling aspects

Fig. 5 shows the boiling curves for water and the 2-propanol/water mixture (3 mol%). The CHF of the 2-propanol/water mixture (2.4MW/m^2) is enhanced 1.6

times compared with the CHF of water (1.5MW/m^2). Fig. 5 also shows the boiling curves for water predicted with the correlation by Stephan and Abdelsalam [12], and for the 3 mol% mixture predicted with the correlation by Fujita and Tsutsui [13]. Fujita and Tsutsui derived an empirical correlation for binary mixtures based on the assumption that the rise in local saturation temperature due to evaporation of the more volatile component leads to decreases in the effective wall superheat, and hence an apparent reduction of the heat transfer coefficient. The boiling curve of water lies close to the results predicted with the correlation by Stephan and Abdelsalam. The boiling curve of the 2-propanol/water mixture shifts toward higher superheat than the boiling curve of water, showing a deterioration in the boiling heat transfer compared with that of water, and agrees fairly well with the results with the correlation by Fujita and Tsutsui. (The heat transfer coefficient of the mixture at the azeotropic point, which is needed to use the Fujita and Tsutsui correlation, was calculated by substituting the thermo-physical properties at the azeotropic point into the Stephan and Abdelsalam correlation.)

Fig. 6 shows the appearance of the boiling for water and the 3 mol% 2-propanol/water mixture at high heat fluxes. At low heat fluxes, the departure diameter of the bubbles are finer and the number of nucleation sites increases by the addition of 2-propanol. At high heat fluxes, large vapor masses covering the heating surface completely are formed with both water and the 2-propanol/water mixture. For the 3 mol% 2-propanol/water mixture, the large vapor masses begin to form at a heat flux around 1 MW/m^2. All of the experimental results shown in the following sections are measured under the high heat flux condition where the large vapor masses are formed on the heating surface.

3.2 Results of temperature measurements

The temperature measurements were carried out over 5.0 s for both water

and the 2-propanol/water mixture, but only the data for the first 1.0 s after the start of the measurements are presented in the following figures (Figs.7 and 8). Fig. 7 shows the temperature traces for boiling in water measured at various heights, h, above the heating surface, at the center of the heating surface (r=0mm) all at a heat flux of 1.0 MW/m^2. At h=0.01 mm and 0.05 mm, the temperature signals exceed the saturation temperature for most of the measurement time, showing that the probe is located within the superheated liquid layer near the heating surface. It is also shown that the downward peaks decrease to the saturation temperature, indicating that saturated liquid and/or vapor exist even in the superheated liquid layer. At h=2.5 mm and 7 mm where the probe tip is inside the vapor masses, the temperature traces become flat with little fluctuation, showing that the vapor masses and the surrounding bulk liquid are in a state of thermal equilibrium.

Fig. 8 shows the temperature traces for the 3 mol% 2-propanol/water mixture measured at various heights over and at the center of the heating surface (r=0mm) at the heat flux of 1.95 MW/m^2. The broken red line is the saturation temperature of the bulk liquid, T_{bp} (89.1℃. Point A in Fig.4), and the chained blue line is the maximum saturation temperature for the bulk liquid of 3 mol% 2-propanol/water mixture, $T_{bp,max}$ (99.7℃. Point C in Fig.4). At h=0.01 mm and 0.05 mm, the upward peaks exceed $T_{bp,max}$, indicating that the probe tip is located in the superheated liquid layer near the heating surface. Further, differing from the cases of water at h=0.01 mm and 0.05 mm, the downward peaks do not fall to T_{bp}, but remains near $T_{bp,max}$ here. At h=0.25 mm, the temperature traces show very small fluctuations, suggesting that the temperatures of the liquid and the vapor are very similar at this location, but the values are considerably higher than T_{bp} and close to $T_{bp,max}$. As the probe location is away from the heating surface (h=1.0, 2.5 mm), the downward peaks approach T_{bp}, and almost agree with

T_{bp} at h=7 mm. The high temperature parts of the signals at h=1.0, 2.5, and 7 mm above the heating surface, which are thought to indicate the vapor temperature inside the vapor masses, remain considerably higher than T_{bp}, the temperature of the vapor equilibrated with the 3 mol% bulk liquid (corresponding to Point C in the phase diagram in Fig.3). Due to this difference between the temperatures inside the vapor masses and the surrounding liquid, the temperature traces at h=1.0, 2.5, and 7 mm show periodic fluctuations, which are thought to correspond to the formation of vapor masses and the inflow of bulk liquid accompanied by the detachment of vapor masses, as will be examined in next two figures (Figs.9 and 10).

As mentioned in detail in the Introduction, the previous paper [7] has measured the liquid-vapor behaviors for 2-propanol/water mixtures using a conductance probe with the same apparatus as that in the present study. Fig. 9-(a) shows an example of the conductance probe signals measured under a condition similar to that in Fig.8: 3mol% 2-propamol/water mixture was boiled at a heat flux of q=2.0MW/m^2, and the conductance probe was placed 3.1mm above the heating surface at the center of the heating surface. The signal level “1” means that the probe tip is in contact with vapor and the signal level “0” that it is in contact with liquid (the wider pulse signals correspond to the vapor mass signals). Fig. 9-(b) shows the power spectrum density (PSD) calculated from the Fourier transform of the probe signals of Fig.9-(a). The sampling interval and the total number of data used for the Fourier transform were 0.1 ms and 32768, respectively. The peaks appear at frequencies around 18-21Hz. Fig. 10 shows the PSD of the temperature fluctuations calculated from the temperature traces at h=1, 2.5, and 7 mm in Fig.8. The sampling interval and the total number of data used for the Fourier transform were the same as the case in Fig.9-(b) (0.1ms and 32768). The PSDs at the three different heights have peaks at frequencies around

18-21Hz, similarly to the case of Fig.9-(b). This result confirms that the periodic fluctuations in the temperature traces at 1, 2.5, and 7 mm in Fig.8 correspond to the formation and detachment of vapor masses, and the high temperature parts of each trace indicate the vapor temperature inside the vapor masses.

Fig. 11 shows the high peak values (the maximum of the upward peaks), T_{max}, the low peak values (the minimum of the downward peaks), T_{min}, and the time averaged value, T_{ave}, of the temperature traces measured at various heights at the heat flux of 1.95 MW/m^2. Fig. 11-(a) has the horizontal axis in linear scale, and Fig.11-(b) in logarithmic scale to show the variation in temperature close to the heating surface more clearly. As the present measurements were carried out at high heat fluxes, the conduction layer adjacent to the heating surface is very thin and could not be detected with the present micro-thermocouple probe. Therefore, the value of T_{max} closest to the heating surface remains lower than the surface temperature, T_w (T_w is 129.8℃ in the case of Figs.11-(a) and (b)). In Fig.11, T_{min} agrees with $T_{bp,max}$ close to the heating surface, then decreases with increasing distance from the heating surface, and agrees with T_{bp}, in the h>3mm region. The T_{max} shows higher values than $T_{bp,max}$ in the superheated liquid region close to the heating surface, then decreases steeply and almost agrees with $T_{bp,max}$ in the h>1 to 2mm region.

Fig. 12 shows semi-log plots of the vertical distributions of T_{min} measured at three different heat fluxes (1.59, 1.95, and 2.23 MW/m^2) at the center of the heating surface, and also T_{min} measured for water at q=1.0 MW/m^2 for reference. For water boiling, the T_{min} at every height agrees with the saturation temperature of the bulk water (100℃). For the 2-propanol/water mixture, T_{min} agrees with T_{bp} at locations far from the surface and increases as the measurement location approaches the heating surface, for all heat fluxes. Further, the T_{min} close to the heating surface tends to approach $T_{bp,max}$ with increasing heat fluxes, but nowhere

exceeds $T_{bp,max}$.

Fig. 13 shows the radial distributions of the temperature, which were measured by traversing the probe horizontally along the centerline of the heating surface. To avoid complicating the graph, only T_{min} is plotted for h=0.1, 0.5, and 2 mm, with both T_{min} and T_{max} plotted for h=7 mm. There are strong non-uniformities in T_{min} at h≤0.5mm: T_{min} is higher than T_{bp} at the central region and falls to T_{bp} near the periphery of the heating surface (r≥4.5mm). This non-uniformity disappears at h=7mm and T_{min} agrees with T_{bp} at all radial locations. The T_{max} at h=7mm agrees with the maximum saturation temperature, $T_{bp,max}$, at the central region, and shows slightly lower values than $T_{bp,max}$ at the periphery of the heating surface.

The results detailed above in Figs. 8 and 11 to 13 clearly indicate that the 2-propanol concentration varies in the vertical and radial directions for the boiling of 2-propanol/water mixture. For boiling of the 2-propanol/water mixtures at high heat fluxes, it would be expected that the local saturation temperature agrees with T_{bp} at locations far from the heating surface, and increases when approaching the heating surface due to the decrease in the 2-propanol concentration. Further, with increasing heat flux, preferential evaporation of 2-propanol becomes more intensive, and hence the local saturation temperature close to the heating surface approaches the maximum value, $T_{bp,max}$, given as point C (x=0.034mol%) in Fig.4 (but it does not exceed the $T_{bp,max}$). These expected variations in the local saturation temperature with the location and the heat fluxes are consistent with the results of T_{min} shown in Figs. 8, 11, and 12. Therefore, it may be possible that the T_{min} of the temperature traces measured at a location can be assumed to be the local saturation temperature of the 2-propanol/water mixture at the same location. In the following section, the local concentration of 2-propanol is estimated based on this assumption.

3.3 Concentration distributions of 2-propanol deduced from T_{min}

Figs. 14 and 15 show the vertical and radial distributions of 2-propanol concentrations estimated from the phase equilibrium diagram using the assumption that T_{min} corresponds to the local saturation temperature of the mixture. Fig.14 is the vertical distribution at the center of the heating surface (r=0mm). For all heat flux conditions, the concentration of 2-propanol agrees with the bulk concentration at regions far from the heating surface and decreases sharply closer to the heating surface. The region where the concentration is smaller than the bulk liquid concentration (3 mol%) tends to expand to positions further from the heating surface as the heat flux increases. Further, at the high heat fluxes of 1.95 and 2.23 MW/m^2 close to the CHF, the concentration of 2-propanol in the close vicinity of the heating surface decreases to the lower limit (0.034 mol%. Point C in Fig.4).

Fig. 15 shows the radial distributions of 2-propnaol concentration at q=1.48 MW/m^2 estimated from the T_{min} shown in Fig.13. Reflecting the T_{min} distributions, the 2-propanol concentrations at h=0.5 mm or nearer decrease considerably in the central region of the heating surface.

In the boiling of 2-propnaol/water mixtures on an upward-facing circular disk, there is bulk liquid inflow from the surrounding areas of the heating surface while the vapor mass is detaching. Then the liquid flows toward the center of the surface accompanying the preferential evaporation of 2-propanol. Consequently, the 2-propanol at the central part of the heating surface becomes more dilute than at the periphery of the heating surface. This is likely the reason why the 2-propanol concentrations show non-uniformity in the radial direction. Further, at the central part of the heating surface, the 2-propanol concentration within the thin liquid layer (macrolayer) beneath the vapor masses is thought to fall to near

the lower 2-propanol concentration limit (0.034 mol%. Point C in Fig.4), and therefore the vapor supplied to the vapor mass due to the evaporation of this liquid layer has a composition similar to that at point B of the phase diagram in Fig.4. This is likely the reason why the temperature inside the vapor masses are very similar to $T_{bp,max}$.

3.4 Estimated surface tension distributions

As detailed in the Introduction, there have been proposals to explain the CHF enhancement of the positive mixtures based on the Marangoni effects induced by surface tension gradients at the liquid-vapor interface. This section evaluates how much non-uniformity can be expected in the surface tension distributions, based on the temperature and the concentration distributions deduced in the preceding sections. With a local saturation temperature, T_{min}, and the corresponding local concentration of 2-propanol, x, the surface tension $\sigma(T_{min}, x)$ was calculated using the empirical correlation in Hoke and Chen [14], who measured the surface tension of 2-propanol/water mixtures in a wide range of concentrations and temperatures.

Fig. 16 shows the calculated vertical distributions of the surface tension at the center of the heating surface (r=0 mm). In Fig.16, σ_A and σ_C are the surface tensions corresponding to point A (x=3 mol%, T_{bp}=89.1°C), and point C (x=0.034 mol%, $T_{bp,max}$=99.7°C) in Fig.4. The surface tension at r=0 mm increases steeply closer to the heating surface, suggesting that a strong Marangoni convection is induced at the liquid-vapor interface. Fig.17 shows surface tension distributions in the radial direction at two heat fluxes, 1.48 and 1.95 MW/m^2. As the temperature measurements were made at only two radial locations r=0 mm and r=4 mm at 1.95 MW/m^2, the data at these two locations are plotted and the two data points are connected with broken lines. These results suggest that radial

non-uniformity becomes significant at higher heat fluxes and nearer the heating surface.

As mentioned in the Introduction, the previous paper [7] established that for the boiling of 2-propanol/water mixtures the macrolayer formed at the center of the heating surface is considerably thicker than that of water, and that the macrolayer thicknesses show a non-uniform distribution in the radial direction, thicker at the central area and thinner near the periphery of the heating surface. The reasons why the macrolayer shows such tendencies have not been satisfactorily explained. According to previous research [15, 16], however, when a bubble generated on a heating surface grows in a liquid with a surface tension gradient similar to Fig.16 (the surface tension increasing toward the heating surface), the Marangoni flow induced around the bubble exerts a force on the bubble promoting the detachment of the bubble from the heating surface. Therefore, when it is assumed that a macrolayer is formed by the coalescence of smaller bubbles generated on the heating surface and that surface tension distributions similar to those in Figs.16 and 17 are formed just after detachment of the preceding vapor masses, promotion of the bubble detachment leads to coalescence of the bubbles at locations further away from the heating surface, further than would be the case in water boiling. This may be one of the causes that a thicker macrolayer is formed at the central part of the heating surface.

Further studies will be needed to fully elucidate the process of macrolayer formation during the boiling of 2-propanol/water mixtures.

4. Conclusions

The temperatures near the heating surface were measured using a micro thermocouple in pool boiling on an upward-facing heating surface for a 3mol% 2-propanol/water mixture at high heat fluxes, and the local concentrations of

2-propanol were deduced based on the measured temperature data. The conclusions obtained by the present study may be summarized as follows:

(1) For water boiling, the low peak values of temperature traces, T_{min}, measured at the center of the heating surface are consistent with the saturation temperature of the bulk liquid. For the boiling 2-propanol/water mixture, the T_{min} at the center of the heating surface varies with the vertical distance from the heating surface: the T_{min} agrees with the saturation temperature of the bulk liquid, T_{bp}, at locations far from the surface, and increases as it approaches the heating surface.

(2) The radial distributions of T_{min} measured close to the heating surface show non-uniform distributions: higher than T_{bp} at the central region and falling to T_{bp} near the periphery of the heating surface

(3) The above results in (1) and (2) clearly indicate that the 2-propanol concentration varies in the vertical and radial directions.

(4) The local concentrations of 2-propanol were estimated by assuming that the low peak value of the temperature fluctuations, T_{min}, corresponds to the local saturation temperature of the mixture. The estimated concentration of 2-propanol at the center of the heating surface decreases steeply toward the heating surface and reaches values near its lower limit (0.034 mol%) in the vicinity of the heating surface at the high heat fluxes near the CHF. This is probably the reason why the temperatures inside the vapor masses are close to the maximum saturation temperature of the bulk liquid, $T_{bp,max}$.

(5) The surface tension evaluated with the local saturation temperature and the local concentration increases steeply near the heating surface at the center of the heating surface. These results suggest that a strong Marangoni convection is induced at the liquid-vapor interface near the heating surface.

References

[1] D.M. McEligot, Generalized peak heat flux for dilute binary mixtures, AIChE, J 10(1964) 130-131.

[2] R.P. Reddy, J.H. Liehnhard, The peak boiling heat flux in saturated ethanol-water mixtures, J. Heat Transfer 111(1989) 480-486.

[3] J.Hovestreudt, The influence of the surface tension difference on the boiling of mixtures, Chem. Eng. Sci. 18(1963) 631-639.

[4] Y. Fujita, Q. Bai, Critical heat flux of binary mixtures in pool boiling and its correlation in terms of Marangoni number, Int. J. Refrig. 20-8(1997) 616-622.

[5] W.M. McGllis, V.P. Carey, On the role of Marangoni effects on the critical heat flux for pool boiling of binary mixtures, J. Heat Transfer 118(1996) 103-109.

[6] V.V.Yagov, Critical heat flux prediction for pool boiling of binary mixtures, Chemical Engineering Research and Design 82(A4) (2004) 457-461.

[7] H. Sakashita, A. Ono, Measurements of Critical Heat Flux and Liquid-Vapor Structure near the Heating Surface in Pool Boiling of 2-propanol/Water Mixtures, Int. J. Heat Mass Transfer 53(2010) 1554-1562.

[8] S.J.D Van Stralen, W.M. Sluyter, Local temperature fluctuations in saturated pool boiling of pure liquids and binary mixtures, Int. J. Heat Mass Transfer 12(1969) 187-198.

[9] M.G. Cooper, C.R. Stone, Boiling of binary mixtures- Study of individual bubbles, Int. J. Heat Mass Transfer 24-12(1981) 1937-1950.

[10] Y. Utaka, S. Sai, An investigation of vapor concentration during boiling of liquid mixture: Measurement of temperature and concentration variation of vapor in bubble, Heat Transfer-Asian Research 31-6(2002) 475-485.

[11] A. Ono, H. Sakashita, Temperature measurements near a heating surface at high heat fluxes in subcooled pool boiling, Heat Transfer-Asian Research 39-1(2010) 27-42.

[12] K. Stephan, M. Abdelsalam, Heat-transfer correlations for natural convection boiling, Int. J. Heat Mass Transfer 20 (1980) 73–87.

[13] Y. Fujita, M. Tsutsui, Int. J. Heat Mass Transfer 37 Suppl. 1 (1994) 291-302.

[14] B.C. Hoke, J.C. Chen, Binary aqueous–organic surface tension temperature dependence, J. Chem. Eng. Data 36 (1991) 322–326.

[15] N.O. Young, J.S. Goldstein, M.J. Block, The motion of bubbles in a vertical temperature gradient, J. Fluid Mechanics 6(1959) 350-356.

[16] S.C. Hardy, The motion of bubbles in a vertical temperature gradient, J. Colloid Interface Sci. 69-1(1979) 157-162.

Captions of figures

Fig.1 Experimental apparatus

Fig.2 (a) Photograph of the micro-thermocouple; and (b) enlargement of the tip of the micro-thermocouple

Fig.3 Phase equilibrium diagram of 2-propanol/water mixtures

Fig.4 Phase equilibrium diagram of 2-propanol/water mixtures in the range of mole fractions of 2-propanol 0 to 0.1

Fig.5 Measured and predicted boiling curves for water and 2-propanol-water mixture (3 mol%)

Fig.6 Boiling appearances of (a) water and (b) 2-propanol-water mixture (3 mol%) at high heat fluxes

Fig.7 Temperature traces for water measured at r=0 mm ($q=1.0$ MW/m^2)

Fig.8 Temperature traces for the 2-propanol/water mixture measured at r=0 mm (3 mol%, $q=1.95$ MW/m^2)

Fig.9 (a) The binary signals of the conductance probe at 3.1 mm above the heating surface and at the center of the heating surface for the 3 mol% 2-propanol/water mixture at $q=2.0$ MW/m^2, (b) Power spectrum density of liquid/vapor signals measured by the conductance probe

Fig.10 Power spectrum densities of temperature fluctuations at h=1, 2.5, and 7 mm, and $q=1.95$ MW/m^2

Fig.11 Maximum, time-averaged and minimum temperatures at r=0 mm. (a)Linear plot, (b) Semi-logarithmic plot

Fig.12 Vertical distributions of T_{min} for different heat fluxes at r=0 mm (Semi-logarithmic plot)

Fig.13 Radial distributions of minimum temperatures (3 mol% of 2-propanol/water mixture, $q=1.48$ MW/m^2)

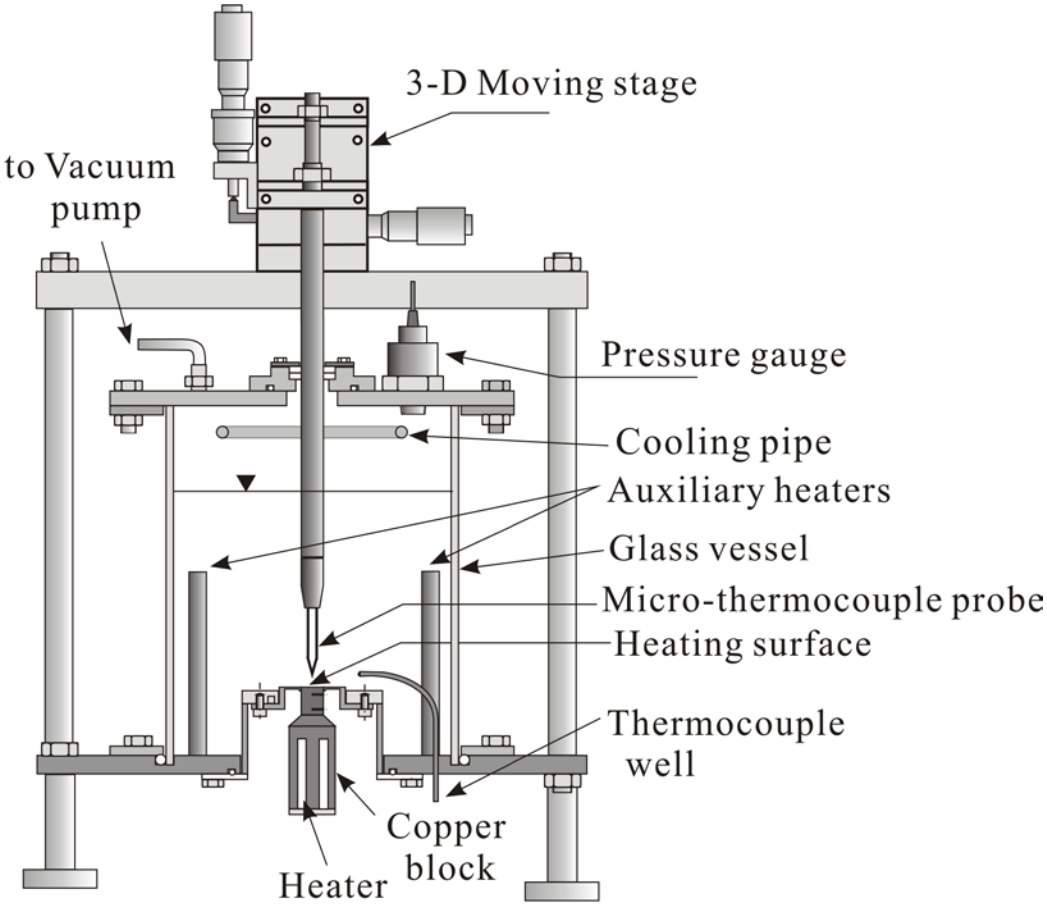

Fig.1 Experimental apparatus

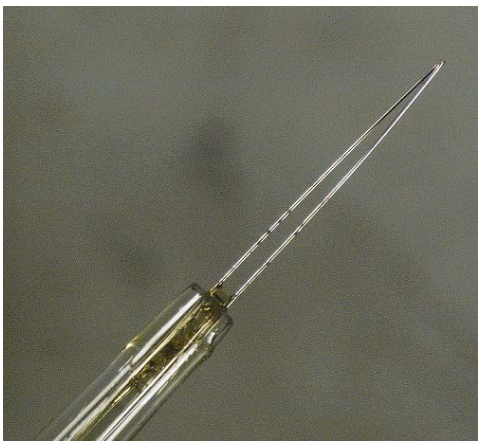

(a)

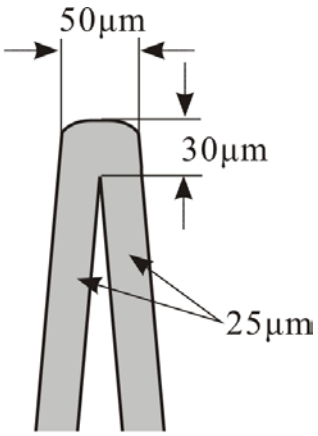

(b)

Fig.2 (a) Photograph of the micro-thermocouple; and (b) enlargement of the tip of the micro-thermocouple

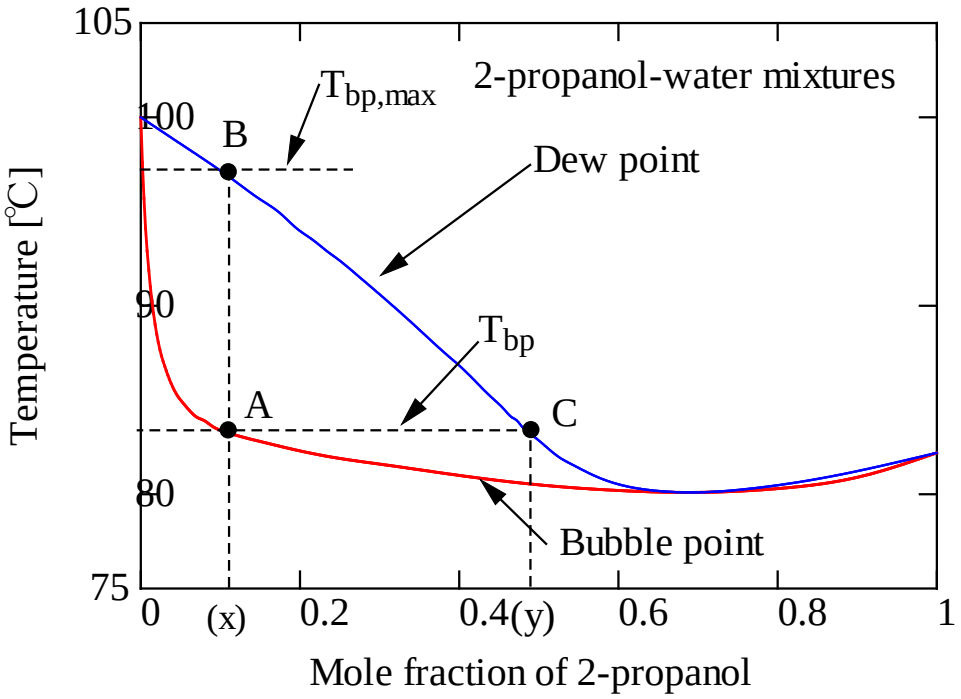

Fig.3 Phase equilibrium diagram of 2-propanol/water mixtures

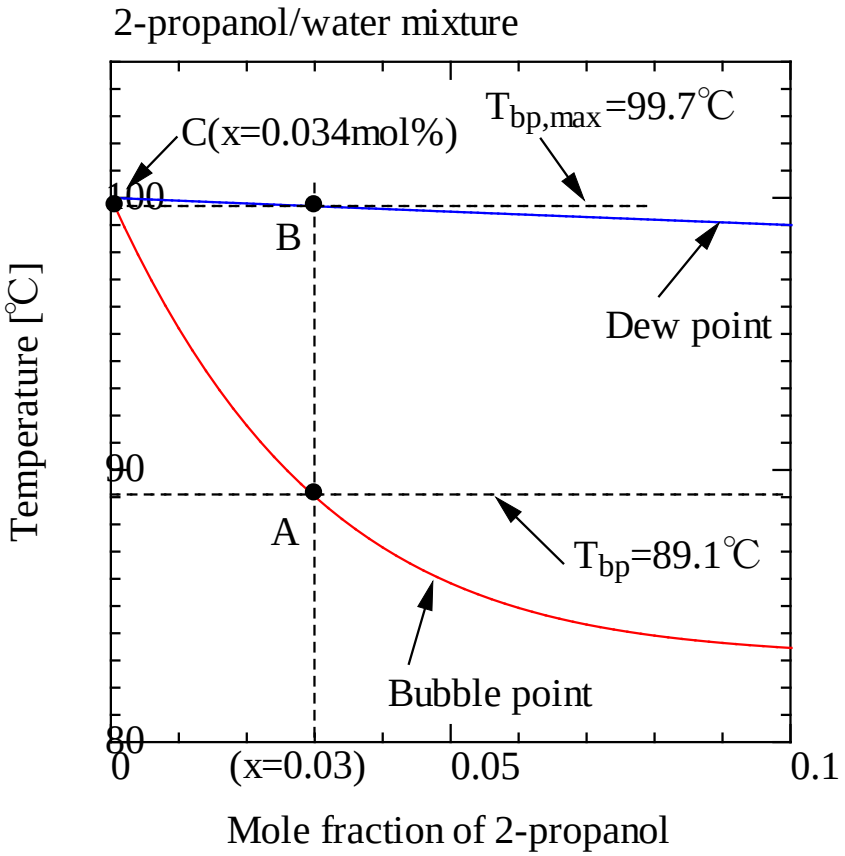

Fig.4 Phase equilibrium diagram of 2-propanol/water mixtures in the range of mole fractions of 2-propanol 0 to 0.1

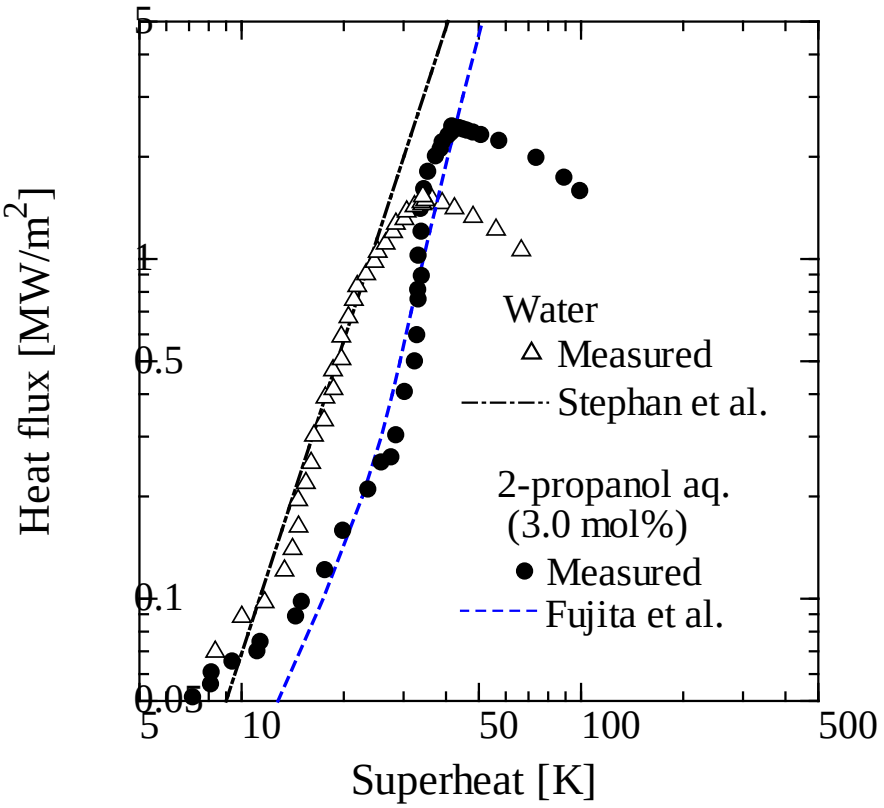

Fig.5 Measured and predicted boiling curves for water and 2-propanol-water mixture (3 mol%)

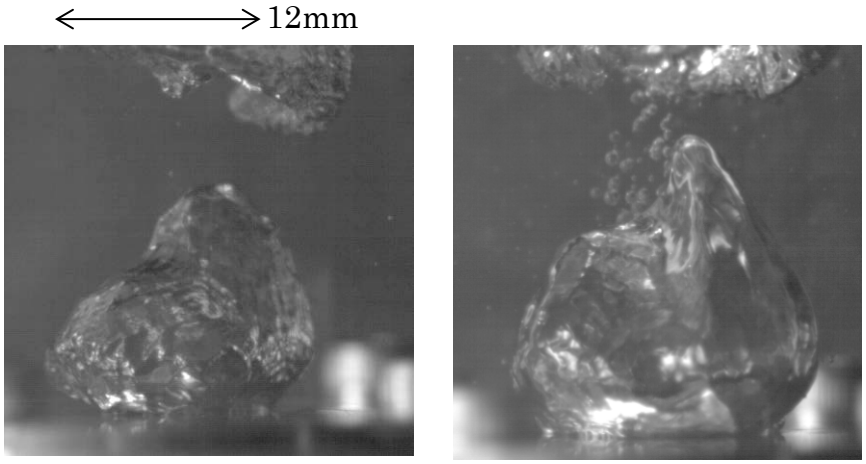

(a) water (q=1.3MW/m^2)

(b) 2-propanol/water mixture (q=1.7MW/m^2)

Fig.6 Boiling appearances of (a) water and (b) 2-propanol-water mixture (3 mol%) at high heat fluxes

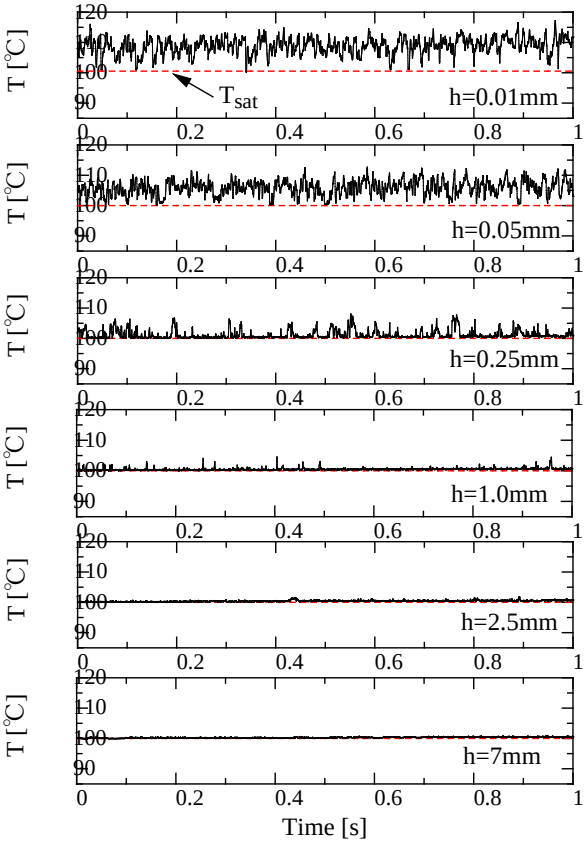

Fig.7 Temperature traces for water measured at r=0 mm (q=1.0 MW/m²)

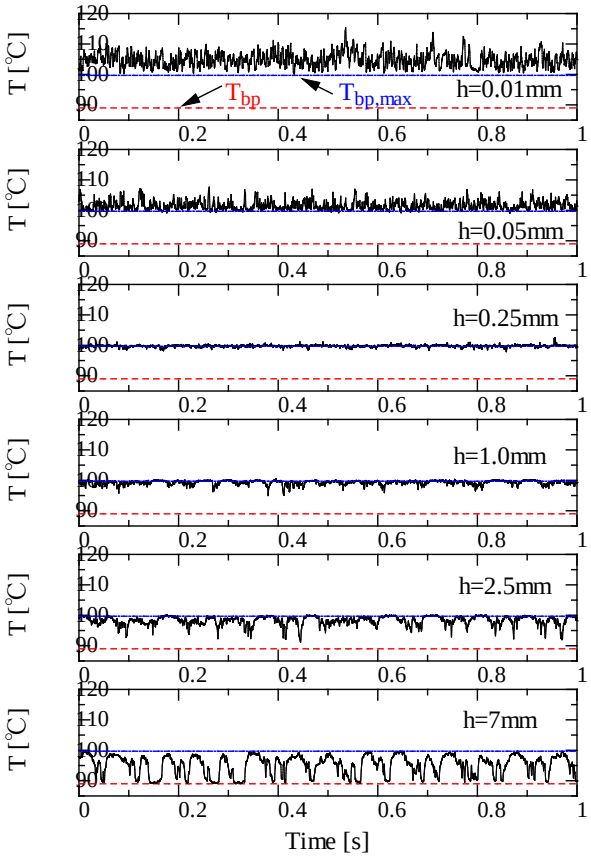

Fig.8 Temperature traces for the 2-propanol/water mixture measured at r=0 mm (3 mol%, q=1.95 MW/m²)

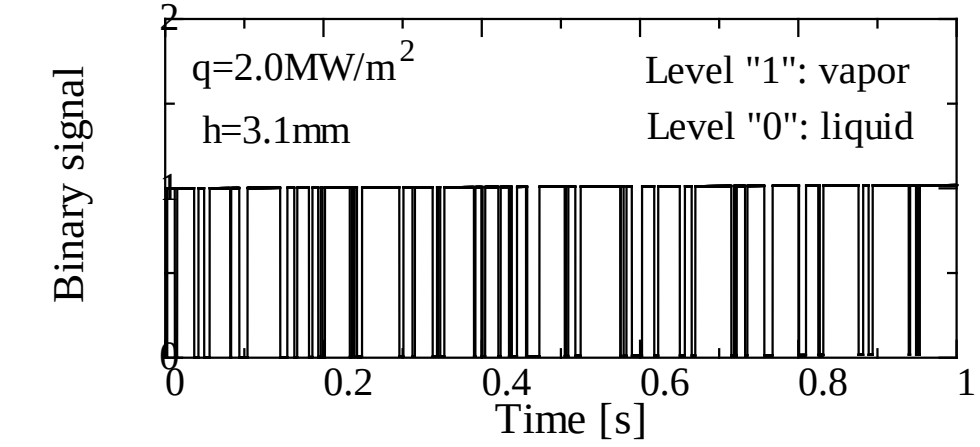

(a)

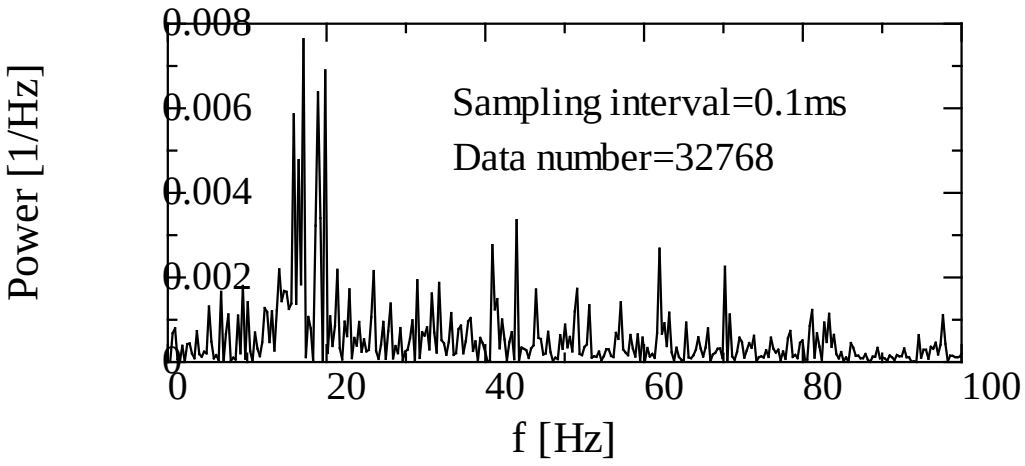

(b)

Fig.9 (a) The binary signals of the conductance probe at 3.1 mm above the heating surface and at the center of the heating surface for the 3 mol% 2-propanol/water mixture at q=2.0 MW/m², (b) Power spectrum density of liquid/vapor signals measured by the conductance probe

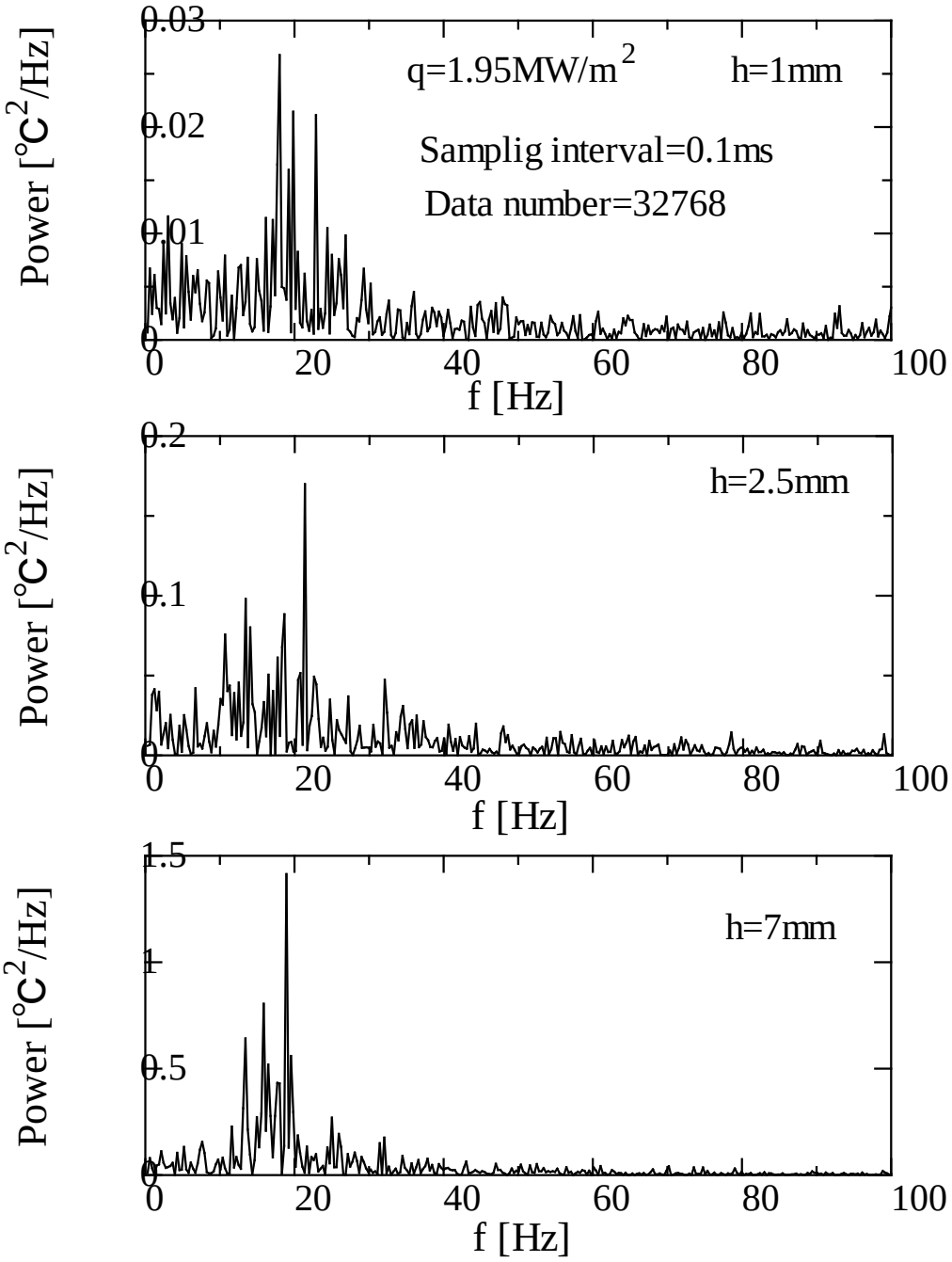

Fig.10 Power spectrum densities of temperature fluctuations at h=1, 2.5, and 7 mm, and q=1.95 MW/m^2

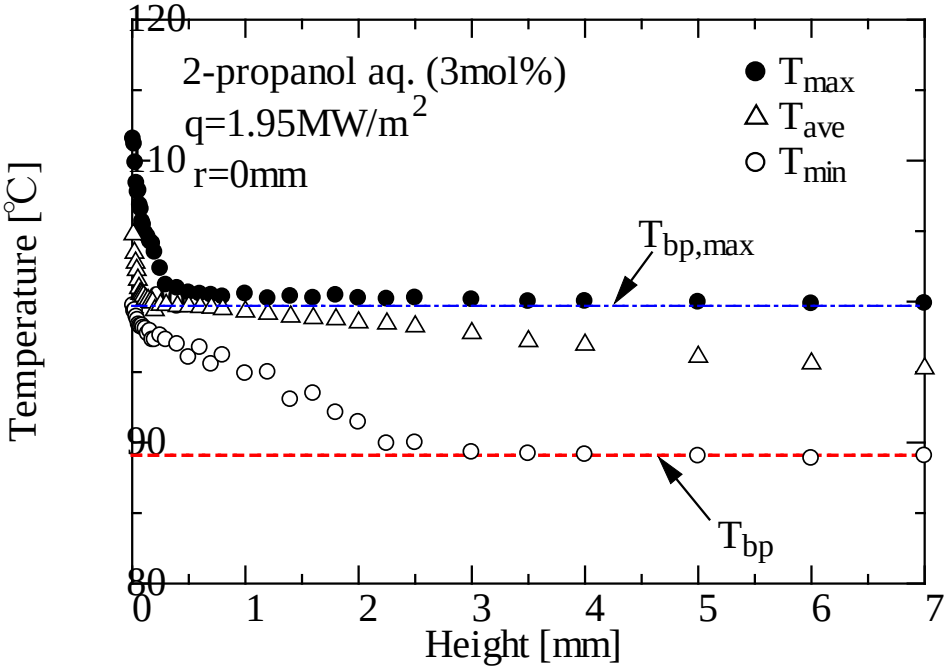

Fig.11-(a)

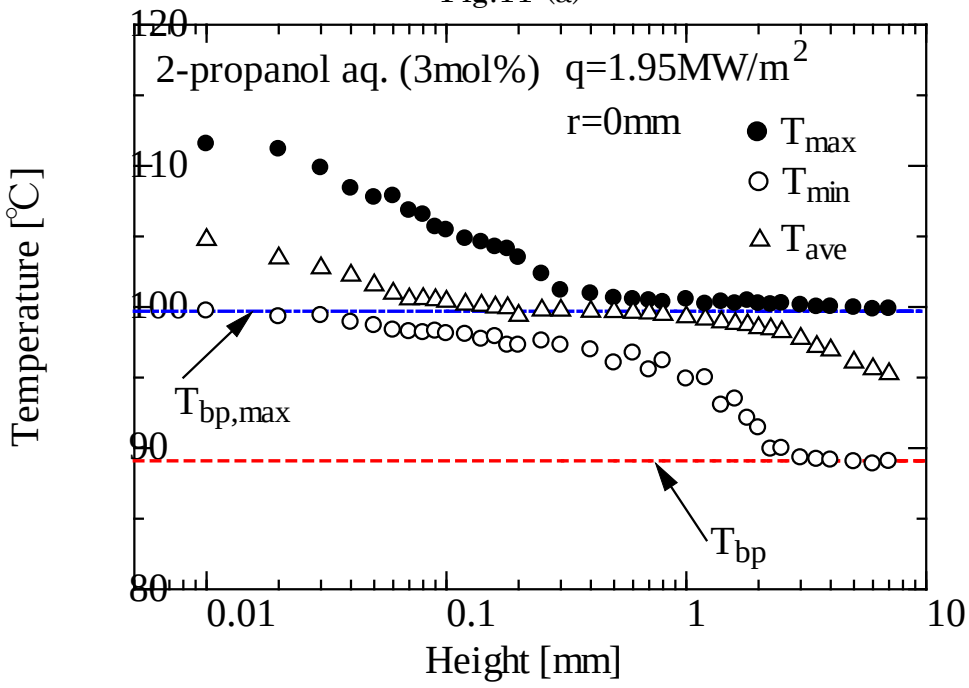

Fig.11-(b)

Fig.11 Maximum, time-averaged and minimum temperatures at r=0 mm.

(a)Linear plot, (b)Semi-logarithmic plot

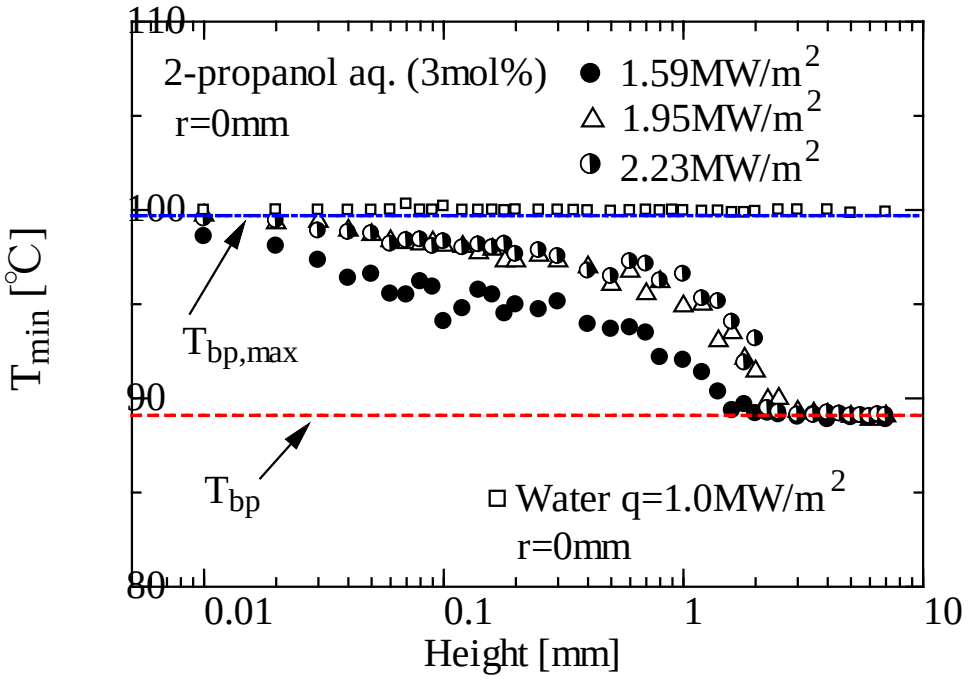

Fig.12 Vertical distributions of T_{min} for different heat fluxes at r=0 mm (Semi-logarithmic plot)

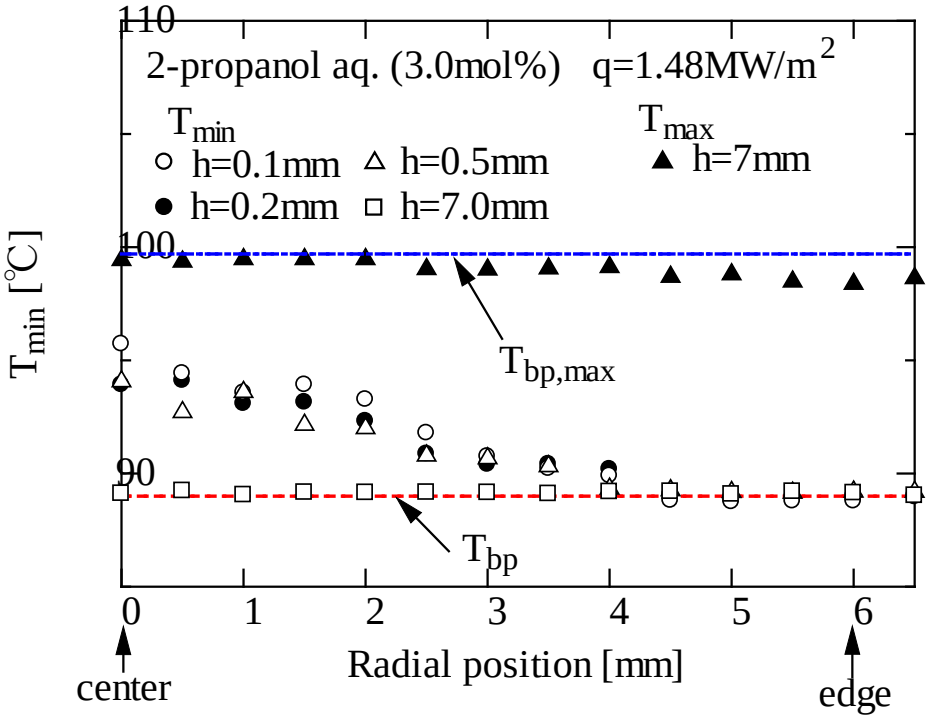

Fig.13 Radial distributions of minimum temperatures (3 mol% 2-propanol/water mixture, q=1.48 MW/m²)

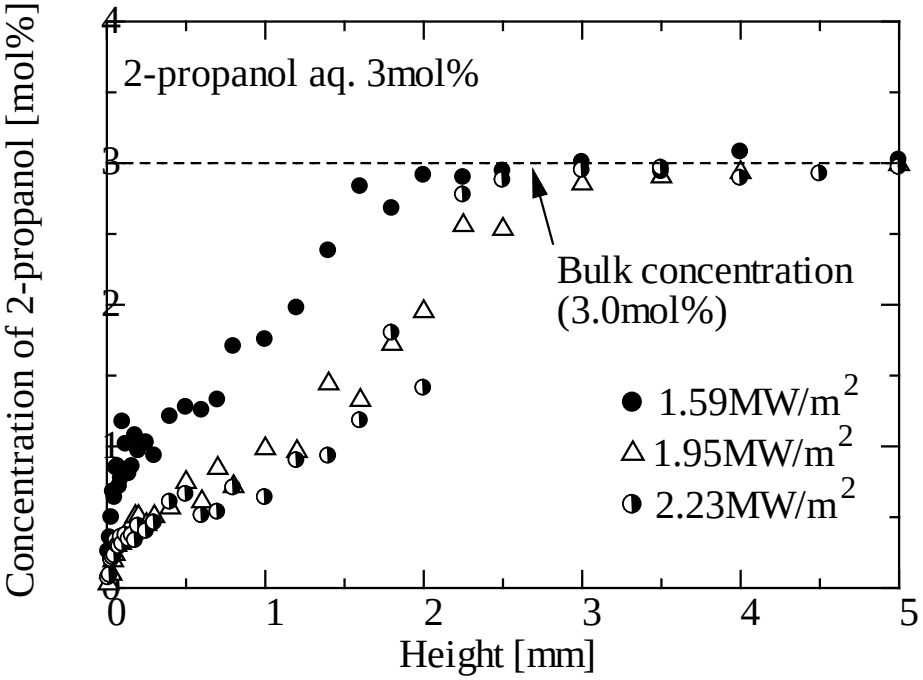

Fig.14 Vertical distributions of 2-propanol concentrations at r=0 mm

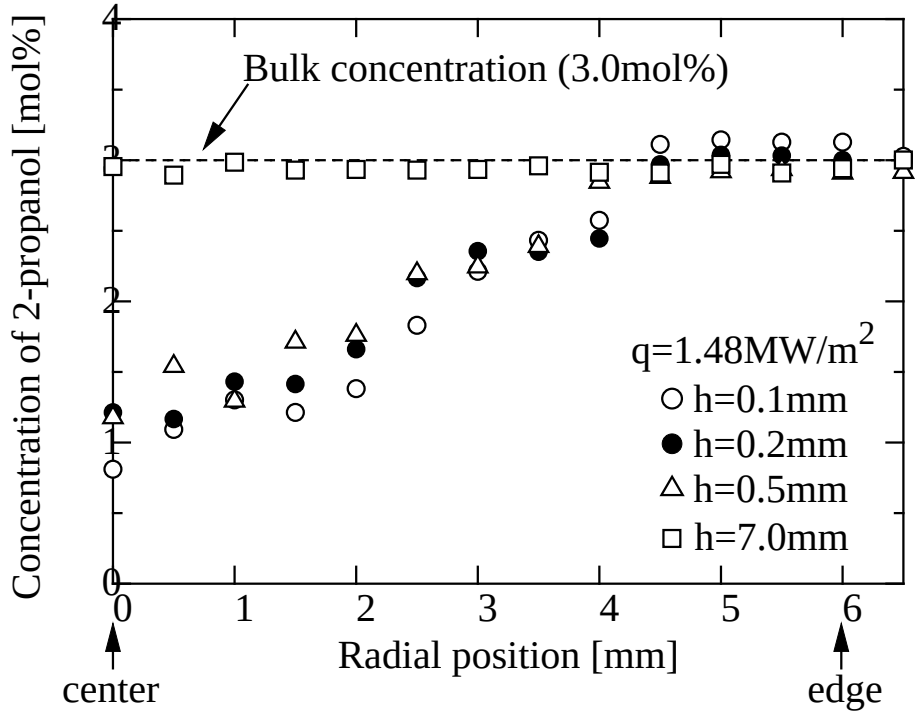

Fig.15 Radial distributions of 2-propanol concentrations

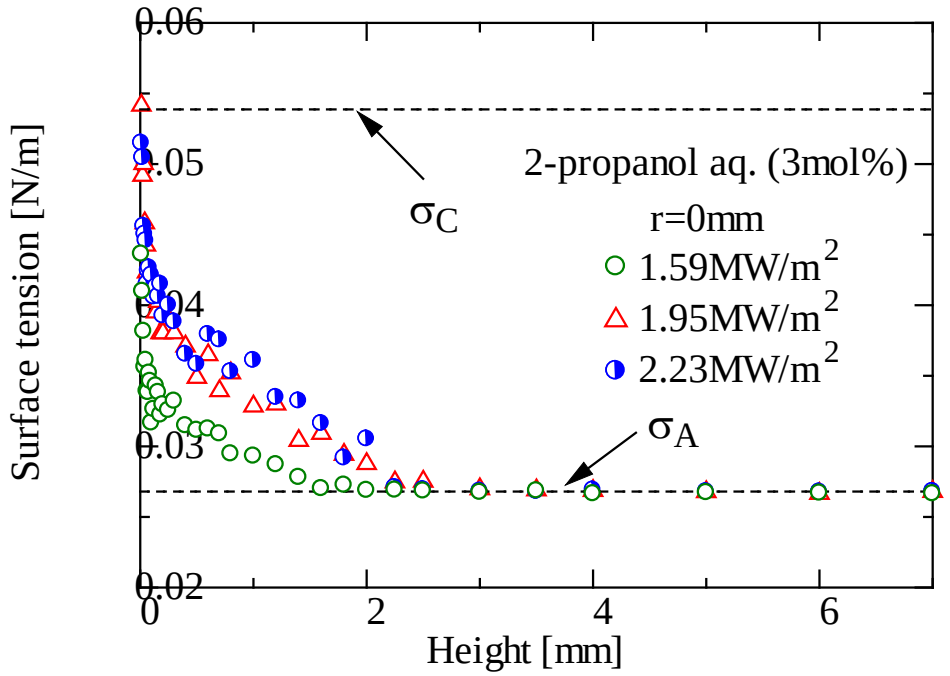

Fig.16 Vertical distributions of surface tension of 2-propanol-water mixture

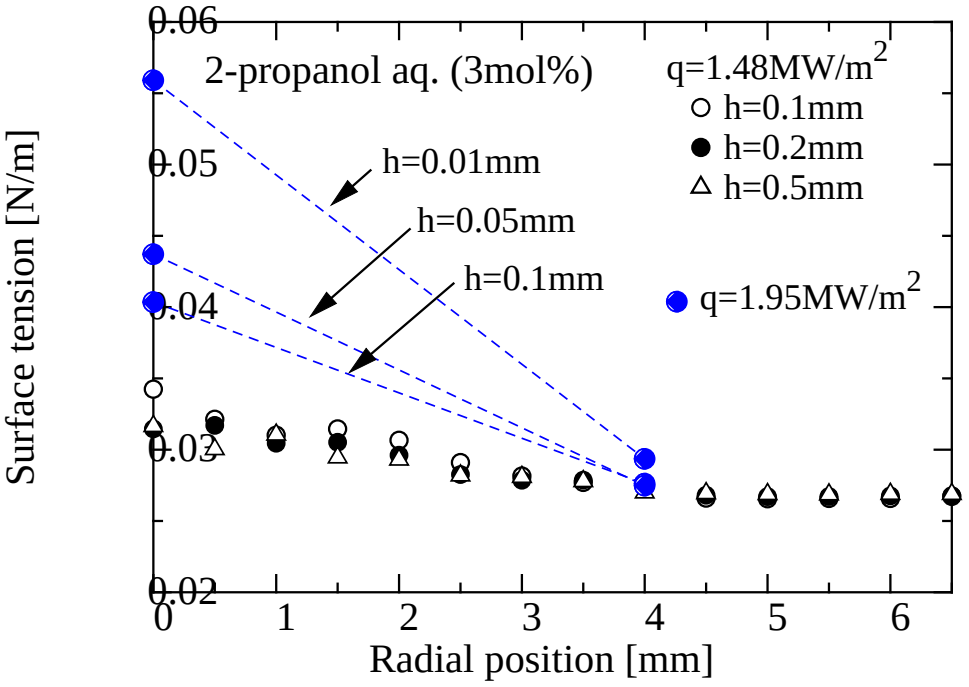

Fig.17 Radial distributions of surface tension of 2-propanol-water mixture